IJRCE

ISSN 2248-9649

International Journal of
Research in Chemistry and Environment

Available online at: www.ijrce.org

Research Paper

Photocatalytic Degradation of Phenol by Polyaniline/ Phosphomolybdic acid/ Poly(vinyl pyrrolidone) Composite under Visible Light

P. Rajesh Anantha Selvan[1], *E. Subramanian[2] and R. Murugesan[3]

[1]Department of Chemistry, St. John's College, Palayamkottai, Tirunelveli-627 002, Tamil Nadu, INDIA
[2]Department of Chemistry, Manonmaniam Sundaranar University, Tirunelveli-627 012, Tamil Nadu, INDIA
[3]Department of Chemistry, TDMNS College, T. Kallikulam, Tirunelveli-627 113, Tamil Nadu, INDIA

(Received 10th August 2017, Accepted 19th September 2017)

Abstract: *Our work is to infusing photocatalytic activity in polyaniline (PANI) by coupling its visible light absorption with the catalytic role of phosphomolybdic acid (PMA), a heteropoly acid. A neutral polymer poly(vinyl pyrrolidone) (PVP) was used as the soft template. By chemical oxidative polymerization method, the four materials viz., PANI, PANI–PVP, PANI–PMA and PANI–PMA–PVP were synthesized. UV-vis, FTIR, XRD and SEM techniques were used to characteristics PANI and its three composite materials. XRD and SEM revealed the interaction of PANI with PMA and PVP. Photocatalytic activity of PANI and its composites was studied by visible light degradation of phenol using Haber inner irradiation photoreactor (λ > 380 nm, irradiation time = 160 min. Experimental parameters for the influence of photocatalytic activity such as initial phenol concentration, pH and dosage of catalyst were investigated. The above four photocatalysts exhibited the phenol photodegradation of 6.8, 10.0, 31.2 and 64.0 % respectively at the optimized condition of initial phenol concentration of 50 mg/L, pH = 6, photocatalyst loading of 0.5 g/L, H_2O_2 2 mL, constant air flow, at room temperature and atmospheric pressure. PANI-PMA-PVP showed the maximum decomposition of phenol. The combined effect of PMA and PVP is believed to play an important role in enhancing the photoreactivity of PANI in visible region.*

Keywords: Chemical polymerization, phenol photodegradation, Phosphomolybdic acid, Polyaniline.

© 2017 IJRCE. All rights reserved

Introduction

Organic-inorganic hybrid materials receive greater attention because of their specific advantageous properties. These new materials have advantages of organic materials such as flexibility, light weight and good malleability, and those of inorganic materials such as stability, high strength, chemical resistance and high reactivity. Polyaniline (PANI)–polyoxometalate (POM) composites combine the mechanical flexibility[1], optical[2] and electrical properties[3] of PANI with the high electrical conductivity[4] and catalytic activity[5] of POM. The incorporation of POM into the PANI matrix offers enhanced performance for both the components[6]. Common methods for combining a polymer with a heteropoly acid (HPA), one of the POMs include (i) electrochemical growth on a support[7], (ii) one-step reaction where the polymer is reacted in solution or on the solid oxidant[8] and (iii) impregrenation of a support material[9]. Recently, more and more attention has been focused on the combination of PANI and phosphomolybdic acid (PMA) photocatalysis[4].

Phenol in waste water is potentially toxic to human, aquatic and microorganism life. Traditional waste water treatment techniques available are activated carbon adsorption[10], chemical oxidative degradation[11], biological digestion[12], etc. However, in each technique there are limitations and disadvantages[11]. The heterogeneous photocatalysis[13], one of the advanced oxidation processes[14], permits the degradation of phenol in aqueous solution in the presence of a photocatalyst. Present investigation applies polyaniline composites photocatalysts for the visible light

degradation of phenol. A neutral polymer, poly (vinyl pyrrolidone) (PVP) was used as a soft template in synthesis. PVP is also a well known steric stabilizer[15]. Composites were prepared by simple conventional aqueous chemical oxidative polymerization[16] of aniline doped with phosphomolybdic acid (PMA- a HPA)[17] and PVP. Binary system PANI-PMA and PANI-PVP composites were prepared by aniline monomer with PMA/PVP. Ternary PANI-PMA-PVP composite was also prepared as a new photocatalyst. The experiments were conducted under visible light in aqueous suspension of photocatalysts, different parameters such as type of catalyst, initial phenol concentration, pH, and dosage of catalyst were also investigated for their influence on phenol degradation. Interesting results are obtained and reported herein.

Material and Methods

PMA was purchased from Sigma-Aldrich and used without further purification. Aniline from Merck was distilled prior to use. Water was used after two distillations (DDW). Con. HCl, PVP, hydrogen peroxide, N-methyl pyrrolidone (NMP) and acetone were obtained from Merck. Sodium carbonate and Folin-phenol reagent were obtained from Spectrum Chemicals.

Synthesis of PANI materials

PANI and its composites were synthesized by chemical oxidative polymerization method[16]. In this method, 2 mL aniline, 2 mL H_2O_2, 2 mL Con. HCl and 94 mL DDW were mixed in a 250 mL beaker and stirred for an hour during the course of polymerization reaction. Then it was allowed to proceed overnight in a refrigerator. After completion of polymerization, the polymer sample formed was filtered with suction, washed several times with 0.1 M HCl, DDW and acetone until the filtrate became colourless. The samples were dried in an air oven at 110°C for about 4 h and ground into fine powder. The polymer sample was stored in air-sealed polythene cover. Similarly PANI-PVP and PANI-PMA were prepared by adopting the same procedure as above with PVP (PANI-PVP: [PVP] = 10 mM) and with PMA (PANI-PMA: [PMA] = 5 mM). The sample PANI–PMA-PVP composite was synthesized by adopting the same procedure as above with 5 mM PMA and 10 mM PVP.

Characterization

The UV-vis spectra of the prepared PANI composites were recorded by a spectrophotometer (Perkin Elmer UV-vis spectrophotometer, Lambda - 25 model) in NMP solvent in quartz cuvettes for the wavelength range of 330–800 nm. The polymer samples were characterized by FTIR spectroscopy. KBr pellets were prepared for the four materials and used to record FTIR spectra with JASCO FTIR - 410 spectrophotometer in the region 400-4000 cm^{-1}. The XRD patterns of all the PANI composites were recorded using a Shimadzu XRD 6000 X-ray diffractometer with Cu-Kα radiation source (λ = 1.54 Å) operated at 40 kV and 30 mA in the 2θ range 10-90° at the scan speed of 10.0° per minute. Microstructure characterization of the polymer samples was made with JEOL JSM-6390 Scanning electron microscope (SEM) operating at 20 kV, after coating the samples with platinum for 45 s using JEOL JFC-1600 auto-fine coater with sputtering technique.

Photocatalysis

The photodegradation studies were carried out in a Haber inner irradiation photoreactor model HIPR LC–150. The light source was the visible light from 150 W tungsten lamp (λ > 380 nm, irradiation time = 160 min, intensity = 14.79 mW/cm^2 at 555 nm measured with Kusem–Meco Luxmeter, model KM Lux 200 K). The photoreactor wall was covered by aluminum foil during the course of reaction. The pH of the medium was adjusted using 0.1 M HCl or NaOH. Air flow at constant rate was made using air pump. The temperature and pressure of the photoreactor was maintained at 28±2°C and atomspheric pressure. 300 mL phenol solution was mixed thoroughly with required quantity of photocatalyst and shaken for 30 minutes to reach adsorption/desorption equilibrium in the absence of light. The initial concentration of phenol was in the range of 10 to 70 mg/L and a catalyst dose of 0.33 to 0.83 g/L was suspended for degradation. Photodegradation study of phenol for the four catalysts PANI, PANI-PVP, PANI-PMA and PANI-PMA-PVP was carried out in light, constant air flow, H_2O_2 2 mL, at initial phenol concentration of 50 mg/L, pH 6, dose of catalyst of 0.5 g/L. Experimental variables like initial phenol concentration, pH and dose of catalyst for phenol degradation were investigated. The first phenol sample from dark equilibrium was taken to determine the initial concentration of phenol. After that tungsten lamp was switched on to start photocatalysis. Samples were taken periodically at various time intervals for 160 min, 2 mL sample was drawn out for every 10 min for an hour and remaining samples were taken at 20 min intervals. The experimental samples were centrifuged and filtered through a Whatman filter paper No.1 to separate catalyst particles.

The percentage of phenol degradation was analyzed by Phenol-Folin method[18]. In this method phenol aliquot was complexed with Folin reagent. By measuring the absorbance at λ_{max} = 650 nm phenol concentrations were determined from the calibration curve (concentration vs absorbance) produced from known concentrations. The percentage photodegradation of phenol was calculated by using equation (1).

$$\% \text{ photodegradation} = (A_0 - A_t)/A_0 \times 100 \quad \text{---------- (1)}$$

Where A_0 and A_t are the absorbances of phenol–Folin complex samples at zero and at time 't' respectively.

Experiments were repeated in duplicate for getting the reproducibility of the results.

Results and Discussion

UV-vis spectral studies

To examine the interaction between PANI, PVP and/or PMA, the UV-vis absorption spectra of the PANI composites in NMP solvent were obtained. They are shown in figure 1 and data in table 1. The spectrum of PANI (figure 1a) consists of three absorption bands[19]. The first one at 380 nm is assigned to π-π* transition, second one at 557 nm to low wavelength polaron-π* (n-π*) transition and another one around 678 nm to a high wavelength polaron-π* transition related to the quinonoid unit, which can be used as a measure of the oxidation state of PANI[19]. However, the π-π* transition band shows a significant blue shift to 369 nm for PANI-PVP composite, low wavelength polaron-π* transition shows a remarkable blue shift to 549 nm, however, the high wavelength polaron-π* transition related to the quinonoid unit is red-shifted to 687 nm[20]. PANI doped with

PMA shows three absorption bands. The first absorption band of PANI-PMA has red-shifted and appears at 394 nm. The PMA in non-reduced form is generally characterized by oxygen-to-metal (O→M) charge transfer bands below 400 nm[7-9] which have mingled with this π-π* band. π-π* transition with red-shift (394 nm) shows the interaction of PMA with the polymer chain[21]. The second and third bands around 553 nm and above 694 nm respectively are also red-shifted and indicate the interaction. In case of PANI-PMA-PVP, by the introduction of PMA and PVP into the PANI matrix, first the relative intensity of π-π* transition is very much enhanced with a considerable blue-shift to 365 nm. This drastic change itself proves the mutual interaction among the components in PANI-PMA-PVP ternary system[8,15,21,22]. Similarly the other two bands also undergo change, indicating this interaction. Considerable increase in absorbance of three component PANI-PMA-PVP sample relative to others definitely indicates that it could be a better photocatalyst than others. Indeed, the extent of light absorption determines the efficiency of any photocatalyst.

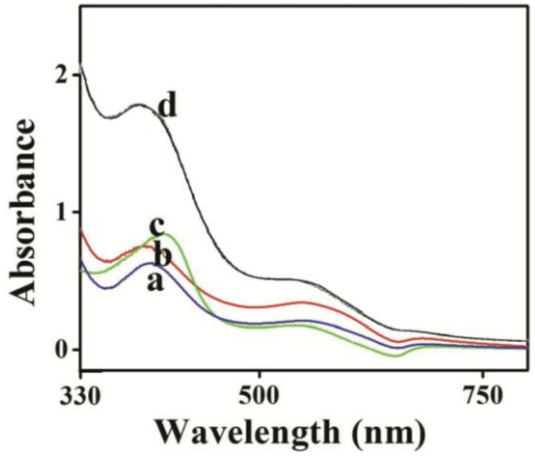

Figure 1. UV-vis spectra of PANI and its composites in NMP solvent
(a) PANI (b) PANI-PVP (c) PANI-PMA and (d) PANI -PMA-PVP

Table 1: UV-vis spectral and XRD data for PANI and its composites

Sample	UV-vis peaks in NMP solvent (nm)	XRD data		
		2θ (deg)	d value (Å)	Average crystallite size (nm)
PANI	380, 557, 678	18.5 25.7	4.79 3.45	13.60 6.90
PANI-PVP	369, 549, 687	28.1	3.19	11.27
PANI-PMA	394, 553, 694	26.4	3.36	105.20
PANI-PMA-PVP	365, 551, 696	26.4	3.36	95.91

FTIR spectral studies

FTIR spectra of PANI and its composites are shown in figure 2. PANI shows the main characteristic bands at 833, 1035, 1186, 1287, 1351, 1442, 1500 and 1566cm^{-1} corresponding to C–H out–of–plane bending vibration for aromatic rings, C-N in-plane bending vibration, (two successive bands), C = N stretching vibration in quinoid, stretching of imine, stretching forms of C–N bond, C=C stretching vibration of benzene ring and C=C stretching vibration of quinoid respectively[19,23]. The spectrum of PANI-PVP composite (figure 2b) moves towards higher wavenumber at 1575 and 1447 cm^{-1}. The red-shifted peak at 1167 cm^{-1} due to C – H in-plane bending shows interaction of PANI with PVP. All the spectral features associated with PANI-PVP composite, especially the shift of peaks indicate strong interaction of PVP[20,24] causing a structural and chemical change in PANI.

FTIR analysis of PANI-PMA (figure 2c) shows peaks at 1569, 1493, 1447, 1287, 1166 and 797 cm^{-1} which are the characteristic peaks of PANI. The bands in the range of 800-1100 cm^{-1} corresponds to PMA which overlap with weak PANI bands in this region. New high intense sharp peak at 1063 cm^{-1} is assigned to stretching mode of P–O bond, peaks at 964 and 853 cm^{-1} are assigned to the Mo=O terminal bond and an symmetric stretching Mo–O–Mo bond, respectively[8,20,25]. Therefore the above IR result shows that PMA is completely interacting with PANI and forms a new composite[20,25]. IR spectra of the ternary composite, PANI-PMA-PVP (figure 2d) exhibit some changes in the bands of the PMA anchored in the polymer matrix as compared to those of the free acid. A detailed inspection of the band of Mo=O group of PMA in the composite shows shifting to 960 cm^{-1} and the band of Mo-O-Mo to 862 cm^{-1}. As could be expected, the inner P-O bonds are affected by the composite formation as indicated by the small variation in frequency of vibrations. The external Mo=O bond stretching shift to lower wave number (960 cm^{-1}) proves the composite formation. But the main changes are observed in Mo-O-Mo vibrations, which involve the more basic oxygen atoms, i.e., those involved in the protonation of the anion. Thus the interaction of PMA and PVP into the polymer matrix is confirmed[26].

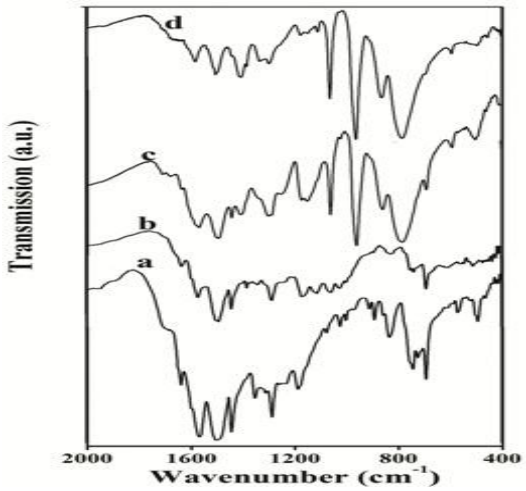

Figure 2: FTIR spectra of (a) PANI (b) PANI-PVP (c) PANI-PMA and (d) PANI-PMA-PVP

XRD studies

The XRD patterns of PANI and its composites are shown in figure 3 and the data commuted are given in table 1. The broad pattern of PANI has the characteristic peaks, first one at 18.5° and second[27] at 25.7° which indicate amorphous nature of PANI. For PANI-PVP composite, the very broad shifted diffraction band at 28.1° shows the incorporation of PVP into PANI matrix. Further, the intensity radio of peaks in PANI (figure 3a) i.e., higher intensity at lower angle peak and lower intensity at higher angle peak, is totally changed in PANI-PVP composite, actually the reverse with peak broadening is observed. These results firmly show the strong interaction between PANI and PVP. XRD pattern of PANI-PVP matched with the reported pattern of PANI[28]. Generally PMA is crystalline in nature and is confirmed from the literature[22]. By the addition of PMA the PANI composites move towards crystalline nature.

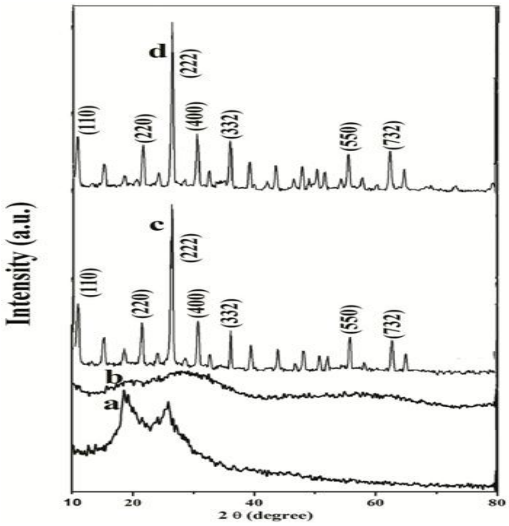

Figure 3: XRD patterns of PANI materials (a) PANI (b) PANI-PVP (c) PANI-PMA and (d) PANI-PMA-PVP

PANI-PMA and PANI-PMA-PVP display sharp peaks (figure 3c and d) at 11.1°, 21.6°, 26.4°, 30.6°, 36.1°, 55.6°, 62.3° and 10.6°, 21.4°, 26.4°, 30.6°, 36.0°, 55.7°, 61.9° respectively. All these peaks were indexed to (110), (220), (222), (400), (332), (552) and (732) set of planes of Primitive Cubic structure with reference to JCPDS File no. 09-0412 for PANI-PMA and JCPDS File no. 09-0412 for PANI-PMA-PVP sample. By comparing PANI-PMA and PANI-PMA-PVP with PANI and PANI-PVP patterns, it is observable that new sharp peaks appear at several positions due to the incorporation of PMA. PMA is dispersed well throughout the PANI polymer matrix without losing its crystalline nature. For PANI-PMA and PANI-PMA-PVP composites, the XRD patterns are in agreement with the previous results[22,29]. For PANI-PMA and PANI-PMA-PVP composites, there is good agreement between the patterns reported in JCPDS files and in Figs. 3c and d in terms of sharp high intense reflections, peak position and (h k l) values of the respective planes. These patterns indicate, beyond any doubt, the presence of crystallinity in PANI-PMA and PANI-PMA-PVP samples. d value decreases from PANI to other composites (table 1) which reveals close arrangement of PANI chains. The intensity of the peaks shows that fine differences do exist between

PANI-PMA and PANI-PMA-PVP in d–space and average crystallite size values. Hence, the soft template PVP and the HPA-PMA mutually interact and also with PANI.

SEM studies

SEM photographs of PANI and its composites taken at 10,000 × magnification are shown in figure 4. PANI has rough-surfaced and irregularly-shaped grains of micron size (figure 4a). PANI-PVP composite has nano rods morphology (figure 4b). The rods have approximately 200 nm dia and few micron lengths. Addition of PVP into PANI as a steric regulator and template has completely changed the morphology of pristine PANI. This is in accordance with our previous work[24]. However, addition of PMA to PANI has changed the PANI morphology into micron size spheres (figure 4c). Primary nano spherical particles agglomerated into secondary clusters are visible in the image in figure 4c. Compared to PANI, the PANI-PMA primary nano spherical particles agglomeration is less and leads to micron size spheres. That means the inorganic PMA is uniformly dispersed in PANI matrix and such observation is consistent with XRD characterization (figure 3c) and was reported in previous study[8] also. The three component composite, PANI-PMA-PVP has entirely different morphology from others (figure 4d) and has almost smooth-surfaced, spherical shaped and uniformly distributed micron-sized particles/grains. These are all secondary particles/clusters consisting of agglomerated nano-sized primary particles.

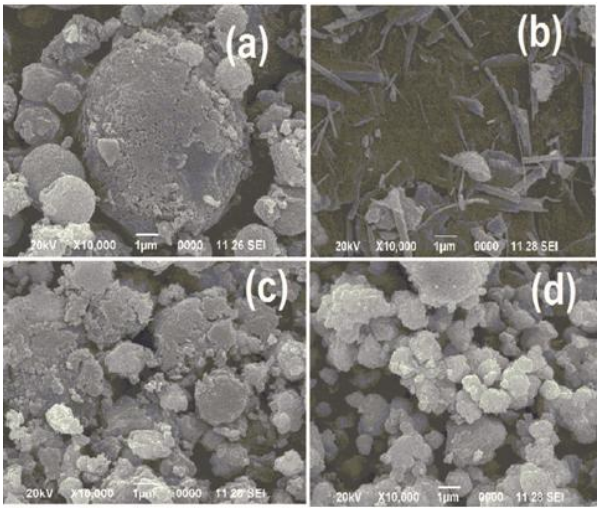

Figure 4: SEM images of (a) PANI (b) PANI-PVP (c) PANI-PMA and (d) PANI-PMA-PVP

One support for this observation is that even those secondary particles have surface-projected nano-size fringes/bristles–like structures which could be visualized on close view (figure 4d). This quite different morphology might have arisen by the mutual interaction between PMA and PVP, thus nullifying the steric control role of PVP. From SEM images one can realize that no separate crystallites of the bulk phase of PMA are found in the composite samples, i.e. they are all homogeneous in nature[30].

Studies of Photodegradation

For preliminary experiment, the photocatalytic degradation of phenol was studied under conditions of a) synthesized catalyst under dark condition and air flow and b) in light, constant air flow and 2 mL H_2O_2 (without catalyst). All these experiments were carried out at initial phenol concentration of 50 mg/L, pH 6 and dose of catalyst of 0.5g/L. The results of the above experiments are displayed in figure 5. There was only negligible degradation (2-3 %) of phenol[31]. That means without catalyst or without the oxidant H_2O_2, phenol decomposition did not take place. The photocatalytic performance of the four catalysts PANI, PANI-PVP, PANI-PMA and PANI-PMA-PVP was investigated in the absence of H_2O_2 under light, [phenol] = 50 mg/L, pH = 6, Temp = 28±2°C, constant air flow and catalyst dose of 0.5 g/L. The results are shown in figure 6. The % degradation of phenol was found to be 4.5, 7.6, 8.8 and 17.0 for the four catalysts respectively. Even without H_2O_2, the catalysts are able to degrade phenol, of course, to a lesser extent. Evidently this result demonstrates that these four materials function as photocatalysts and could produce reactive oxygen species like $^{\bullet}OH$, $O_2^{\bullet-}$ etc., with aerial O_2 or H_2O_2.

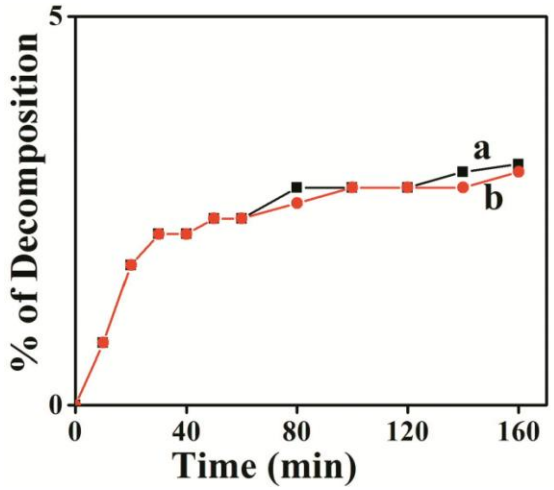

Figure 5: Photocatalytic degradation of phenol (a) in dark in the presence of PANI and air flow (without oxidant H_2O_2) and (b) in light, constant air flow and 2 mL H_2O_2 (without catalyst PANI)

Also addition of PVP and/or PMA to PANI enhances the latter's activity. Particularly, the combination PMA-PVP works better and the resulting catalyst PANI-PMA-PVP exceedingly has a higher efficiency

than others. In the above experiment, however, if H_2O_2 was added, the degradation results could be far better. This is investigated in further experiments.

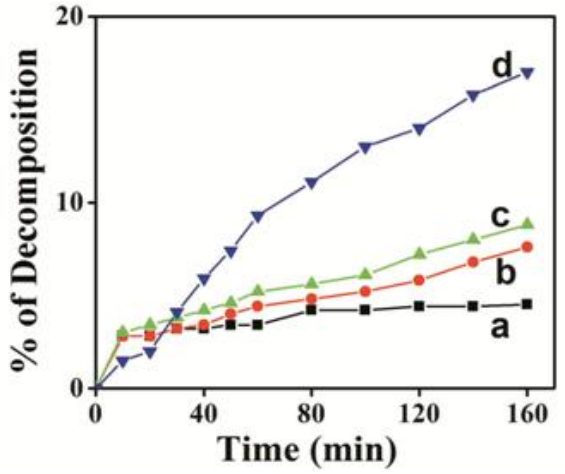

Figure 6: Photocatalytic performance of (a) PANI (b) PANI-PVP (c) PANI-PMA and (d) PANI-PMA-PVP in phenol degradation

Condition: [phenol] = 50 mg/L, pH = 6, Temp = 28±2°C, catalyst dose = 0.5 g/Land constant air flow (no H_2O_2).

Effect of types of catalyst with H_2O_2

The photocatalytic degradation of phenol in the presence of PANI, PANI – PVP, PANI – PMA and PANI–MA–PVP are found to be 6.8, 10.0, 31.2 and 64.0 % respectively at optimized conditions as shown in figure 7.

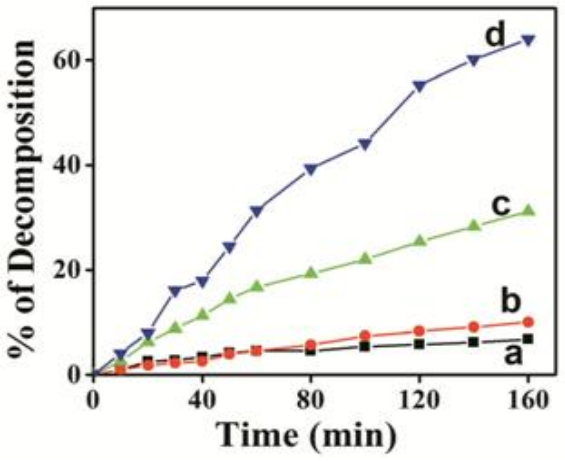

Figure 7: Photocatalytic performance of (a) PANI (b) PANI-PVP (c) PANI-PMA and (d) PANI-PMA-PVP in phenol degradation

Condition: [phenol] = 50 mg/L, pH = 6, temp = 28±2°C, catalyst dose = 0.5 g/L, H_2O_2 = 2 mL and constant air flow.

On comparing the efficiency of the catalysts without and with H_2O_2 (2 mL addition and incorporation into 300 mL phenol reaction solution) (figure 6 and 7), it is inferable that there is enhancement in efficiency with H_2O_2, particularly to a greater level for the last two catalysts PANI-PMA and PANI-PMA-PVP. Such observation is already reported[32]. Addition of external oxidant H_2O_2 to the heterogeneous system improves the formation of hydroxyl radicals and hence the degradation extent[32]. In PANI-PMA-PVP it enhances the photodegradation by 3.7 times.

Effect of initial phenol concentration

The influence of initial phenol concentration plays a vital role for photodegradation of phenol[31-33]. The effect of initial phenol concentration at various levels of 10, 30, 50 and 70 mg/L was investigated and the degradation data are plotted in figure 8. Photocatalytic degradation increases with increase in initial phenol concentration from 10 to 30 mg/L reaches a maximum value at 50 mg/Land then decreases at higher concentration (70 mg/L) and the degradation data are 2.66, 14.1, 32.0 and 15.47 mg/L respectively. So, 50 mg/L is the optimal phenol concentration for its maximal degradation. The decrease in degradation at higher phenol concentration (70 mg/L) is explained as follows. At higher phenol concentration, equilibrium adsorption of phenol on the catalyst surface, increases[34]. As a result, competitive adsorption of H_2O_2/O_2 on the same site decreases and consequently the amount of •OH and O_2•$^-$ formed on the surface of catalyst decreases. This leads to a decrease in degradation efficiency.

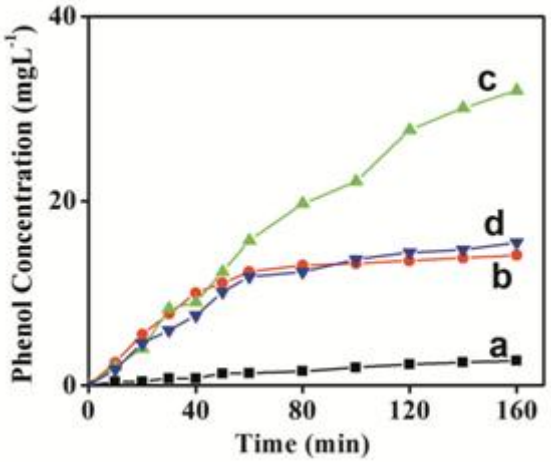

Figure 8: Effect of initial phenol concentration (mg/L) on degradation (a) 10 (b) 30 (c) 50 and (d) 70.

Condition: pH = 6, Temp = 28±2°C, dose of PANI-PMA-PVP = 0.5 gL^{-1}, H_2O_2 = 2 mL and constant air flow

Effect of pH

pH is an important factor for phenol degradation[35]. The role of pH on the efficiency of phenol removal

from solution was investigated in the pH range of 2.0 to 8.0, the results are plotted in figure 9. After 160 min reaction time, the % degradation obtained are 25.3, 32.0, 64.0 and 16.2 at pH = 2.0, 4.0, 6.0 and 8.0 respectively. The maximum degradation occurred at a pH of 6.0 and the lower degradation occurred at pH = 2.0 and 8.0.

The point of zero charge (pH_{zpc}) of the PANI–PMA–PVP catalyst was found to be 6.97, an almost neutral pH. At highly acidic pH 2.0, the surface charge of the catalyst is positive, since H^+ can be attached to aniline group. This is an unfavorable situation. While at pH 8.0, the catalyst surface may be negative. Since pKa of phenol is 11, at higher pH 8, the proportion of availability of phenoxide ion will be increasingly higher. Hence there could be electrostatic repulsion between phenoxide and catalyst, which renders phenol adsorption difficult. Altogether pH 6.0 is a conducive condition for maximum adsorption of phenol and is, thus the optimal pH condition. A similar observation has been noted in previous studies[35,36].

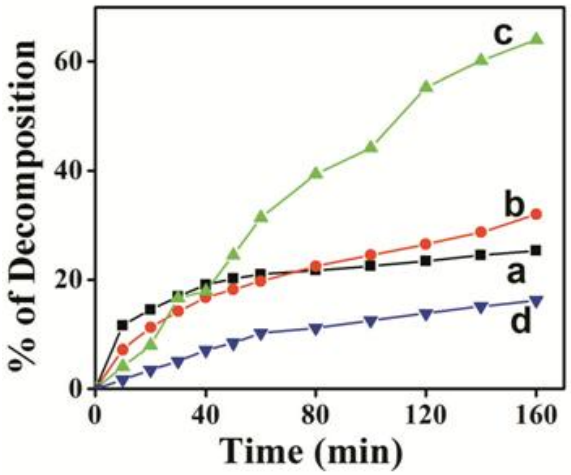

Figure 9: Effect of pH on photodegradation of phenol (a) 2 (b) 4 (c) 6 and (d) 8

Condition: [phenol] = 50 mg/L, Temp = 28±2°C, dose of PANI-PMA-PVP = 0.5 g/L, H_2O_2 = 2 mL and constant air flow

Effect of the dose of catalyst

To study the effect of catalyst dose on phenol degradation, a dosage variation of 0.33 to 0.83 g/L of the optimized catalyst PANI-PMA-PVP was employed. The results in figure 10 show that the percentage of phenol degradation increases with increasing catalyst loading upto 0.5 g/L (maximum decomposition of 64.0 %) and then decreases. The observed initial increase in degradation efficiency might be due to the increase in the number of active sites on the photocatalyst surface. The decrease in degradation efficiency observed beyond the catalyst loading of 0.5 g/L could be attributed to the increase in turbidity of the solution as a result of the excess catalyst present in the phenol solution. This leads to the so called screening effects[37,38] that involves the reflectance, interception and scattering of light and hence incident light rays could not penetrate into the solution. From our findings, the catalytic loading increase will increase the number of photons absorbed, the available active sites and consequently the concentration of phenol molecules adsorbed. However, an optimum is reached where light penetration is compromised because of excessive particle concentration. The tradeoff between these two opposing phenomena results in an optimum catalyst loading[34,37,38] for the photocatalytic degradation.

From the parametric variation study described in Sections 3.5.1-3.5.4, it is concludable that PANI-PMA-PVP is the highest efficient catalyst which functions better at the optimized condition of 50 mg/L phenol concentration, pH 4.0, and a dosage of 0.5 g/L.

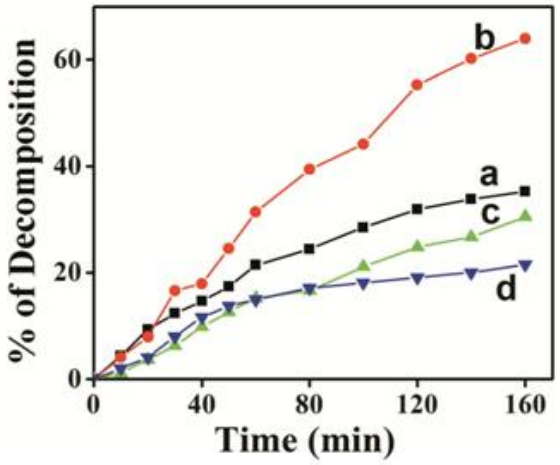

Figure 10: Effect of PANI-PMA-PVP catalyst dosage (g/L) on phenol destruction (a) 0.33, (b) 0.5, (c) 0.67 and (d) 0.83

Condition: pH = 6, [phenol] = 50 mg/L, Temp = 28±2°C, H_2O_2 = 2 mL and constant air flow.

UV-Vis spectra during phenol degradation

Degradation of phenol was confirmed by the change in UV-Vis absorption spectrum of phenol. Uv-vis spectrum of phenol as a function of time in presence of PANI–PMA–PVP catalyst under visible light illumination is shown in figure 11. It is evident that absorption peak of phenol at 270 nm[39] decreases with time. Higher catalytic activity occurred during the first 100 min reaction time and after that the catalysis occurred at a slower but constant rate and hence the phenol pollutant is mineralized. The gradual decrease in absorption at 270 nm without the appearance of any new peak confirms phenol degradation[39].

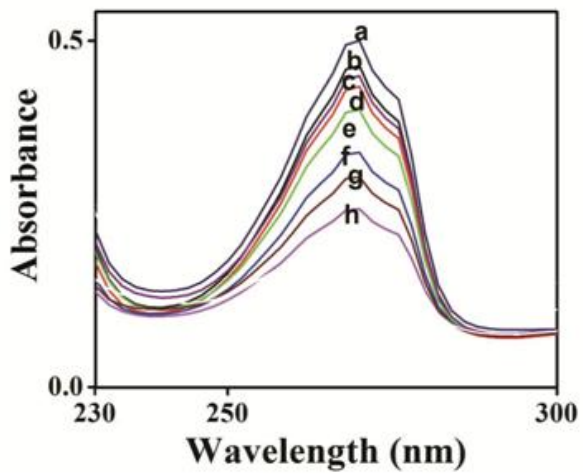

Figure 11: UV-vis spectrum of phenol during its photodegradation with PANI-PMA-PVP at various time intervals of (a) 20 min (b) 40 min (c) 60 min (d) 80 min (e) 100 min (f) 120 min (g) 140 min and (h) 160 min

Condition: [phenol] = 50 mg/L, Temp = 28±2°C, catalyst dose = 0.5 g/L, H_2O_2 = 2 mL and constant air flow

Conclusion

The binary and ternary PANI composites, PANI–PVP, PANI–PMA and PANI–PMA–PVP were prepared by chemical polymerization method. UV-vis and FTIR showed the formation of new composites by the interaction of PVP/PMA with PANI. X-ray diffraction and SEM studies confirmed that the first two were amorphous and the remaining were nanocrystalline in nature. The results on phenol degradation showed that PANI-PMA-PVP photocatalyst, at a dosage of 0.5 g/L, pH = 6 and initial phenol concentration of 50 mg/L under visible light degraded 64 % of phenol after 160 min. The photodegradation study, thus, suggests that the light absorption of PANI and catalytic role of PMA could be coupled for high photocatalytic functionality. The soft template, PVP facilitated the role through small particle formation and active sites number enhancement. This work opens a new avenue for the design of new modified photocatalysts with high activity for the large-scale water treatment and other applications.

References

1. Da-Wei Wang. F., Li. J., Zhao W., Ren, Zhi-Gang Chen. J., Tan, Zhong-Shuai Wu. I., Gentle. G.Q., Lu, and Hui-Ming Cheng, Fabrication of grapheme/polyaniline composite Paper via In Situ Anodic electropolymerization for High-performance flexible electrode. *ACS nano.*, **3(7):** 1745-1752 **(2009)**

2. Leon P.D., Campbell S.A., Smith J.R. and Walsh F.C., Conducting polymer coatings in electrochemical technology Part 2- Application areas. *Trans. Inst. Met. Finish.*, **86(1)**: 34-40 **(2008)**

3. Hu Y. and Gao J., Cationic effects in polymer light-emitting electrochemical cells. *Appl. Phys. Lett.*, **89**: 253514-1 **(2006)**

4. Herrmann S., Ritchie C. and Streb. C., Polyoxometalate-conductive polymer composites for energy conversion, energy storage and nanostructured sensors. *Dalton Trans*., **44**: 7092-7104 **(2015)**

5. Ren Y., Wang M., Chen X., Yue B. and He H., Heterogeneous catalysis of Polyoxometalate based Organic-Inorganic hybrids. *Materials*, **8**: 1545-1567 **(2015)**

6. Katsoulis D.E., A Survey of applications of Polyoxometalates. *Chem. Rev*., **98**: 359-387 **(1998)**

7. Casan-Pastor N. and Gomez-Romero P., Polyoxometalaates: From inorganic chemistry to Materials science. *Front. Biosci*., **9**: 1759-1770 **(2004)**

8. Papagianni. G. G., Stergiou. D. V., Armatas. G. S., Kanatzidis. M. G., and Prodromidis. M. I., Synthesis, characterization and performance of polyaniline-polyoxometalates (XM_{12}, X = P, Si and M = Mo, W) composites as electrocatalysts of bromates. *Sensors and Actuators B*., **173**, 346-353, **(2012)**

9. Lefebvre F., Synthesis, characterization and applications in catalysis of Polyoxometalate/Zeolite composites. *Inorganic*, **4(13)**: 1-24 **(2016)**

10. Ma Y., Gao N., Chu W., and Li C., Removal of phenol by powdered activated carbon adsorption. *Front. Environ. Sci. Eng*., **7(2)**: 158-165 **(2013)**

11. Ukiwe L.N., Egereoun U.U., Njoku P.C., Nwoko I.A. and Allinor J.I., Polycyclic Aromatic Hydrocarbons degradation techniques: A Review. *Int. J. Chem*., **5(4)**: 1-13 **(2013)**

12. Fang H.H.P., Liang D.W., Zhang T., and Liu Y., Anaerobic treatment of phenol in wastewater under thermophilic condition. *Water Research*, **40**: 427-434 **(2006)**

13. Rajeshwar K., Chenthamarakshan C.R., Goeringer S. and Djukic M., Titania-based heterogeneous

photocatalysis. Materials, mechanistic issues and implications for environmental remediation. *Pure Appl. Chem.*, **73(12)**: 1849-1860 **(2001)**

14. Jabeen S., Ali R., Hany O., Amir M. and Khan M.A., Advanced oxidation process for phenol degradation by UV/TiO_2 in aqueous solutions. *Bull. Env. Pharmacol. Life Sci*., **3(12)**: 143-148 **(2014)**

15. Zhang Y., Wang Y. and Yang P., Effects of chloride ions and poly(vinyl-pyrrolidone) on morphology of silver particles in solvothermal process., *Adv. Mat. Lett*., **2(3)**: 217 **(2011)**

16. Kavitha B., Kumar K.S. and Narsimlu N., Synthesis and characterization of polyaniline nano-fibers., *Indian J Pure and Appl. Phys*., **51**: 207-209 **(2013)**

17. Ren Y., Yue B., Gu M. and He H., Progress of the application of mesoporous Silica-supported Heteropolyacids in heterogeneous catalysis and preparation of nanostructured Metal Oxides. *Materials*, **3**: 764-785 **(2010)**

18. Blainski A., Lopes G.C. and Palazzo de Mello. J.C., Application and analysis of the Folin Ciocalteu Method for the determination of the total phenolic content form *Limonium brasiliense* L., *Molecules*, **18**: 6852-6865 **(2013)**

19. Gajendran P. and Saraswathi R., Polyaniline-carbon nanotube composites. *Pure Appl. Chem.*, **80(11)**: 2377-2395 **(2008)**

20. Gu L., Zhao X., Tong X., Chen J.M.B., Liu S., Zhao H., Yu H. and Chen J., Facile preparation of polyaniline nanoparticles and their dispersion for waterborne anticorrosion coatings. *Int. J. Electrochem. Sci*., **11**: 1621-1631 **(2016)**

21. Gong J., Cui X.J., Wang S.G., Xie Z.W. and Qu. L.Y., A novel synthesis of polyaniline doped with heteropolyacid and its special property. *Chinese Chem. Lett.*, 1**3(2):** 123-124 **(2002)**

22. Almeida L.C.P., Goncalves A.D., Benedetti J.E., Miranda P.C.M.L., Passoni. L.C. and Nogueira A.F., Preparation of conducting polyanilines doped with Keggin-type polyoxometalates and their application as counter electrode in dye-sensitized solar cells. *J. Mater. Sci*., **45**: 5054-5060 **(2010)**

23. Shukla S.K., Bharadvaja A., Tiwari A., Parashar G.K. and Dubey G.C., Synthesis and characterization of highly crystalline polyaniline film promising for humid sensor, *Adv. Mat. Lett*., **1(2)**: 129-134 **(2010)**

24. Murugesan R., Anitha G., Subramanian E., Multi-faceted role of blended poly(vinyl pyrrolidone) leading to remarkable improvement in characteristics of polyaniline emeraldine salt. *Mater. Chem. Phys*., **85**: 184-194 **(2004)**

25. Lira-Cantu M., Gomez-Romero P., Electrochemical and chemical synthesis of the Hybrid Organic-Inorganic electroactive material formed by Phosphomolybdate and Polyaniline. Application as cation-insertion electrodes. *Chem. Mater*., **10**: 698-704 **(1998)**

26. Posudievsky O.Y., Kurys Y.I. and Pokhodenko V.D., 12-Phosphormolybdic acid doped polyaniline-V_2O_5 composite. *Synth. Met*., **114:** 107-111 **(2004)**

27. Nadaf L.I. and Venkatesh K.S., Polyaniline-Copper Oxide nano-composites: Synthesis and characterization. *Mat. Sci. Res. India*., **12(2)**: 108-111 **(2015)**

28. Ray D.K., Himanshu A.K. and Sinha T.P., Structural and low frequency dielectric studies of conducting polymer nanocomposites. *Indian J. Pure and Appl. Phys.*, **45**: 692-699 **(2007)**

29. Alothman Z.A., Alam M.M., Naushad M. and Bushra R., Electrical conductivity and thermal stability studies on polyaniline Sn(IV) tungstomolybdate nanocomposite cation-exchange material: Application as Pb(II) Ion-selective membrane electrode. *Int. J. Electrochem. Sci*., **10:** 2663-2684 **(2015)**

30. Popa A., Plesu N., Sasca V., Kis E.E. and Marinkovic-Neducin R., Physicochemical features of polyaniline supported heteropolyacids. *J. Optoelectron. Adv. M*., **8(5)**: 1944-1950 **(2006)**

31. Choquette-Labbe M., Shewa W.A., Lalman J.A., and Shanmugam S.R., Photocatalytic degradation of phenol and phenol derivatives using Nano-TiO_2 catalyst: Integrating quantitative and qualitative factors using response surface methodology. *Water*, **6**: 1785-1806 **(2014)**

32. El-Hamshary H., El-Newehy M.H., Al-Deyab S.S., Oxidation of phenol by hydrogen peroxide catalyzed by Metal-containing Poly(amidoxime) grafted starch. *Molecules*, **16**: 9900-9911 **(2011)**

33. Fufa T.O., Mengesha A.T., Yadav O.P., Photocatalytic activity of nanopolyaniline(NPA)

on phenol degradation. *Afr. J. Pure Appl. Chem.*, **10(3)**: 33-41 **(2016)**

34. Montanez J.P., Gomez S., Santiago A.N. and Pierella L.B., TiO_2 supported on HZSM-11 zeolite as efficient catalyst for the photodegradation of chlorobenzoic acids. *J. Braz. Chem. Soc*., **26(6)**: 1191-1200 **(2015)**

35. Poznyak T., Tapia R., Vivero J. and Chairez I., Effect of pH to the decomposition of aqueous phenols mixture by ozone. *J. Mex. Chem. Sic*., **50(1)**: 28-35 **(2006)**

36. Tasic Z., Gupta V.K. and Antonijevic M.M., The mechanism and kinetics of degradation of phenolics in wastewaters using electrochemical oxidation. *Int. J. Electrochem. Sci*., **9:** 3473-3490 **(2014)**

37. Osarumwense J.O., Amenaghawon N.A. and Aisien F.A., Heterogeneous photocatalytic degradation of phenol in aqueous suspension of periwinkle shell ash catalyst in the presence of UV from sunlight. *J. Eng. Sci. Tech*., **10(12):** 1525-1539 **(2015)**

38. Chen X., Liang Y., Zhou X. and Zhang Y., Phenol removal by a novel non-photo-dependent semiconductor catalyst in a pilot-scaled study: Effects of initial phenol concentration, light, and catalyst loading. *J. Nanomater*., **ID: 457485**, 1-8 **(2014)**

39. Darzi J. and Simin Visible light photodegradation of phenol using nanoscale TiO_2 and ZnO impregnated with Merbromin Dye: A mechanistic investigation. *Iran. J. Chem. Eng*., **33(2)**: 55-64 **(2014)**.